Earth, Planets and Space

FULL PAPER

Open Access

Multi-parametric observations of intermittent hydrothermal water discharge in West Crater of Iwo-Yama volcano, Kirishima Volcanic Complex, Japan

Harutou Tanabe[1*], Takeshi Matsushima[2], Koki Aizawa[2] and Dan Muramatsu[1,3]

Abstract

From April to July 2021, West Crater at Iwo-Yama, Kirishima Volcanic Complex, Japan, was repeatedly filled with hydrothermal water and subsequently evacuated. The overall cycle lasted 14–70 h, and the course of a single cycle followed this sequence of phases: (i) steam effusion disappeared 20–40 min before hydrothermal water discharge; (ii) hydrothermal water discharge occurred, generating a hydrothermal water pool; (iii) steam effusion resumed and gradually increased; and (iv) drain-back (evacuation) of the hydrothermal water occurred 1–1.5 h before the onset of the next hydrothermal water discharge. We used multi-parametric observations (optical camera, thermometer, electric self-potential (SP) electrodes, seismometer, acoustic sensor, and tiltmeter) to investigate the cause of the cyclic hydrothermal water discharge. A change in SP data occurred approximately 2 h before the onset of hydrothermal water discharge. However, the change in SP was small when hydrothermal water discharge did not occur. The temporal change in SP is inferred to have been caused by groundwater flow through the region below West Crater, implying that groundwater flow was occurring 2 h before hydrothermal water discharge. The polarity of SP change suggests that groundwater flowed toward the region underlying the vents. Seismic signals in the frequency range of < 20 Hz decreased 15–45 min after the onset of change in SP. This seismic signal pattern is inferred to have been caused by bubble activity in boiling fluid. We interpret that the inflow of cold groundwater inhibited boiling activity in the conduit, which in turn caused the cessation of both steam effusion and seismic activity. SP data suggest that the inflow of cold groundwater gradually decreased before hydrothermal water discharge. Pressurization sufficient to force the water in the upper part of the conduit to ascend could have built up in the lower part of the conduit owing to a decrease in the input of groundwater into the upper part of the conduit and the continuing supply of steam bubbles and hot water. This increase in pressure finally led to hydrothermal water discharge at the surface. We suggest that the inflow of cold groundwater into the geyser conduit was the key control on the occurrence and cyclicity of hydrothermal water discharge in West Crater at Iwo-Yama.

Keywords Geyser, Electric self-potential, Electric field, Multi-parametric observations

*Correspondence:
Harutou Tanabe
haruto_tanabe@kyudai.jp
Full list of author information is available at the end of the article

Graphical Abstract

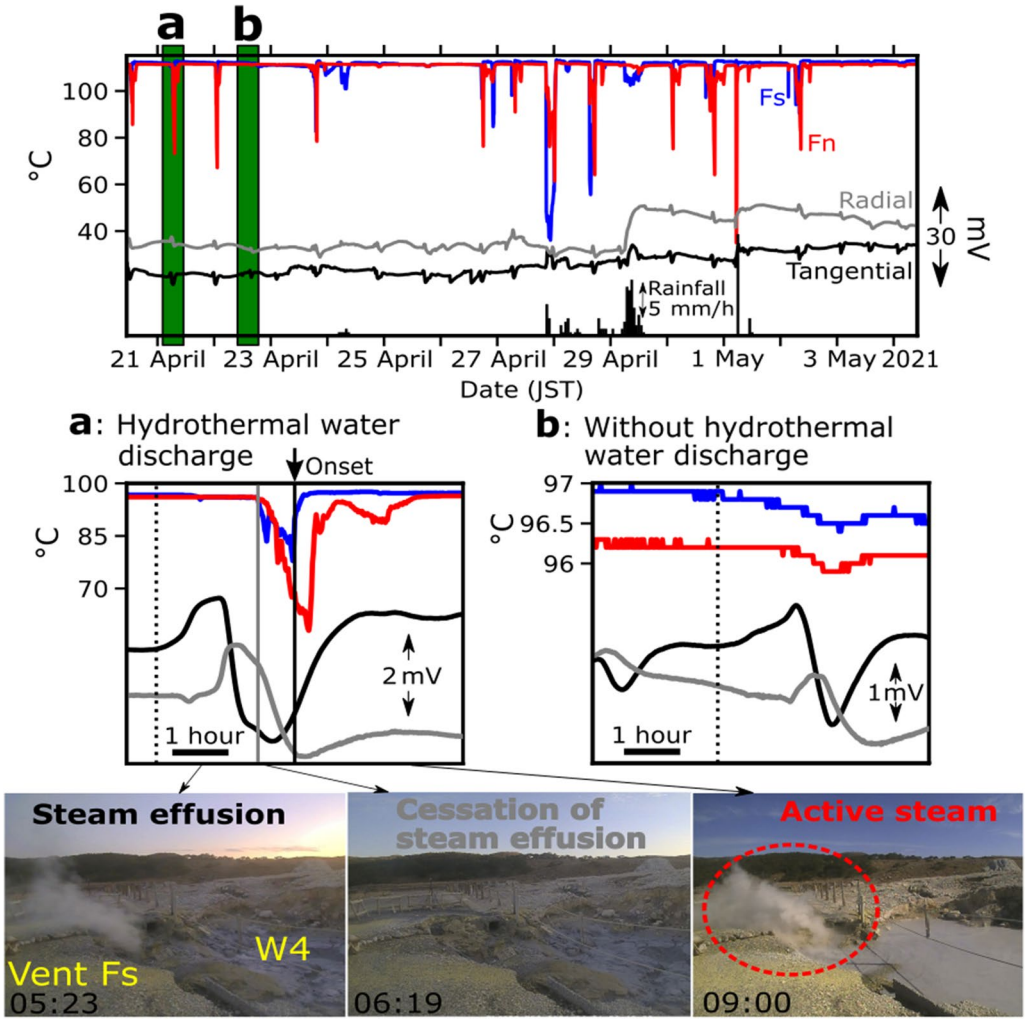

Introduction

A geyser is a type of hot spring that intermittently discharges hydrothermal water and steam. Geyser eruptions are characterized by a regular interval and duration and therefore show similarity to the cyclicity of Strombolian-type eruptions and volcanic tremor (e.g., Kieffer 1984; Nishimura et al. 2006; Hurwitz et al. 2021). However, the study of geyser eruptions has advantages over the study of volcanic eruptions, as the former are smaller than the latter and occur more frequently. Therefore, geyser eruptions provide an opportunity to collect more observational data near the vent (Hurwitz and Manga 2017; Hurwitz et al. 2021). Experimental studies are also helpful for understanding the diverse discharge style involved in geyser activity (Ingebritsen and Rojstaczer 1993; Toramaru and Maeda 2013; Adelstein et al. 2014; Namiki et al. 2016). The study of geysers has the potential to improve our understanding of volcanic eruptions by collecting data over a large number of eruption cycles (Nishimura et al. 2006; Vandemeulebrouck et al. 2014).

Geysers are rare, numbering fewer than 1000 worldwide (Bryan 1995). Each geyser has its particular style of eruption and eruption duration and interval (frequency), and these properties constitute the most basic information for understanding geyser activity (e.g., Manga and Brodsky 2006; Hurwitz et al. 2008; Namiki et al. 2014; Eibl et al. 2020). Examples of geyser eruption duration and interval include those for Onikobe geyser, Japan (50–100 s eruption duration with 10 min interval; Nishimura et al. 2006) and Old Faithful geyser,

USA (2–5 min duration with 30–100 min interval; Kedar et al. 1996). Strokkur geyser, Iceland, shows a mean eruption frequency of 7 min and is unique in that it has one to six eruptions in one event (Eibl et al. 2020). At Strokkur, water fountains for multiple eruptions are spaced an average of 16.1 s apart, and the mean interval between events is 3.7 min after a single eruption to 16.4 min after sextuple eruptions (Eibl et al. 2020). For geysers in Yellowstone National Park, USA, it has been suggested that the change in eruption interval is related to climate change and/or seismic events (Manga and Brodsky 2006; Hurwitz et al. 2008).

Geyser formation is favored in regions with sufficient water supply, an underground fracture network (e.g., provided by landslides), and a low-permeability cap that prevents fluid ascent (Hurwitz and Manga 2017). The mechanism of geyser eruption has been studied since the nineteenth century. Mackenzie (1811) proposed that the plumbing system for a geyser includes an underground cavity termed a "bubble trap", whereby ascending steam bubbles are trapped in the cavity, and a subsequent pressure increase causes the geyser to erupt. Bunsen (1847) suggested that the plumbing system comprises a simple long vertical pipe, with eruptions being caused by decompression boiling in the conduit resulting from overflow. The structure of geyser bubble traps has attracted increasing research attention in recent years. For example, Belousov et al. (2013) described underground bubble trap structures from video observations of geyser conduit interiors in Geyser Valley, Kamchatka, Russia. Adelstein et al. (2014) characterized the bubble trap structure and its importance to upper-conduit heat transfer from visual observations and temperature measurements of a laboratory model.

The mechanism of geyser eruptions has been investigated using various observational methods and modes. In addition to visual imaging in geyser conduits (e.g., Belousov et al. 2013), geophysical observations at the surface have been conducted around geysers. For example, the measurement of temperature (e.g., Nishimura et al. 2006; Eibl et al. 2021) and pressure (e.g.,Kedar et al. 1996, 1998) in the conduit, seismic tremor (e.g., Kieffer 1984; Kedar et al. 1996, 1998; Cros et al. 2011; Vandemeulebrouck et al. 2013; Wu et al. 2017, 2019, 2021), tilt motion (e.g., Nishimura et al. 2006; Vandemeulebrouck et al. 2014; Eibl et al. 2021), and acoustic waves (e.g., Nishimura et al. 2006; Johnson et al. 2013; Vandemeulebrouck et al. 2014). Measurements at geyser sites have revealed that water temperature increases at the time of geyser eruption (Nishimura et al. 2006; Eibl et al. 2021). Acoustic wave measurements of fountain-type geysers have shown that the timing of an eruption and its duration can be estimated from acoustic signals (Nishimura et al. 2006; Johnson et al. 2013). Seismic signals recorded at Old Faithful Geyser in Yellowstone National Park, which has a vent opening of approximately 2 m × 1 m, are generated by bubble activity (i.e., the growth, collapse, or movement of bubbles) in boiling fluid within the geyser conduit (e.g., Kieffer 1984; Kedar et al. 1996, 1998; Vandemeulebrouck et al. 2013; Wu et al. 2019). At Old Faithful Geyser in Yellowstone and Strokkur Geyser in Iceland, two locations of seismic sources have been reported, representing the reservoir and conduit (Cros et al. 2011; Vandemeulebrouck et al. 2013; Eibl et al. 2021). Measurements of tilt motion at Onikobe Geyser in Japan, which has an eruption interval of about 10 min and an eruption duration of 50–100 s, reveal vent uplift before eruptions and subsidence during eruptions (Nishimura et al. 2006).

Electromagnetic data have also been collected from geysers and crater lakes (Nishi et al. 2000; Legaz et al. 2009a and b; Lupi et al. 2022). Legaz et al. (2009b) reported a change in resistivity structure synchronous with water level fluctuations at Inferno Crater Lake in New Zealand. Cyclic changes in electric self-potential (SP) have also been observed around geysers (Nishi et al. 2000; Legaz et al. 2009a). Change in SP occurs via an electrokinetic mechanism by the flow of groundwater through porous media (e.g., Ishido and Mizutani 1981; Aizawa et al. 2009). Therefore, SP provides information about local subsurface groundwater flow that cannot be estimated from other geophysical observations. However, in geysers, it is unclear what kind of groundwater flow induces change in SP and what mechanism triggers the groundwater flow.

In this study, we performed multi-parametric observations using an optical camera, thermometer, electric SP electrodes, seismometer, acoustic sensor, and tiltmeter. The observational target was the intermittent hydrothermal water discharge and associated processes in West Crater of Iwo-Yama, Kirishima Volcanic Complex, Japan (Fig. 1a). The hydrothermal water discharge at Iwo-Yama started abruptly in April 2021 and stopped in July 2021. Similar sudden activation of geysers has been reported for Shinyu hot spring geyser, Shaman geyser in Russia, and Steamboat geyser in Yellowstone, USA (Fukui et al. 2020; Kiryukhin and Karpov 2020; Reed et al. 2021), although the cause of the sudden change in hydrothermalism has not been identified for these sites. Our study acquired a unique dataset extending from the initiation to termination of geyser activity, on which basis we were able to identify groundwater flow as the mechanism of the intermittent hydrothermal water discharge.

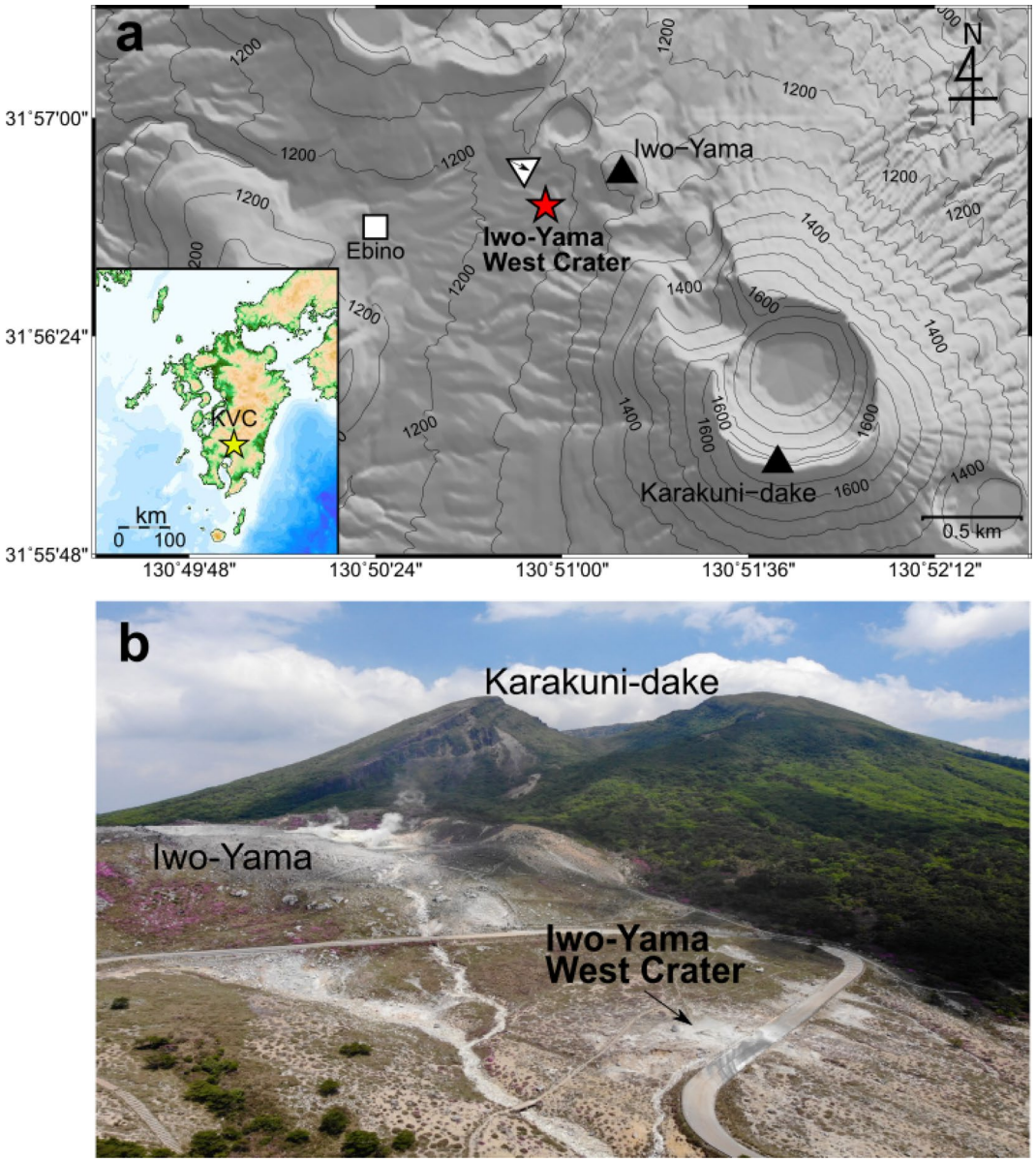

Fig. 1 Map of the Kirishima Volcanic Complex (KVC) and Iwo-Yama. **a** Location of Iwo-Yama West Crater (red star). The white square shows the location of the Ebino rainfall observation site of the Japan Meteorological Agency. The inset shows the location of the KVC. Topographic contours are in meters. **b** Aerial photograph of Iwo-Yama volcano and West Crater taken by a drone device on 29 May 2020 from the location shown by the white triangle in panel **a**

Hydrothermal activity at Iwo-Yama West Crater

Iwo-Yama is one of several active cones of the Kirishima Volcanic Complex (KVC) on southern Kyushu Island, Japan (Fig. 1a). At Iwo-Yama, a phreatic eruption occurred on 19 April 2018, and geothermal activity at the volcano is known to have been essentially continuous since around AD 1900. The geology of Iwo-Yama includes a debris avalanche deposit generated by phreatic eruptions at Karakuni-dake located southeast of Iwo-Yama (Fig. 1) at 4.3 ka (Tajima et al. 2014). Iwo-Yama volcano underwent a small phreatic eruption starting at 15:39 on 19 April in Japan Standard Time (JST: UTC + 9 h), forming several new craters (Tsukamoto et al. 2018; Tajima et al. 2020; Aizawa et al. 2022), including (on 20 April) a new crater to the west of Iwo-Yama (Iwo-Yama West Crater; Muramatsu et al. 2021; Fig. 1). A hot spring pool with an active fumarole has existed in West Crater (hereafter referred to as "W4"; Fig. 2) since the formation of

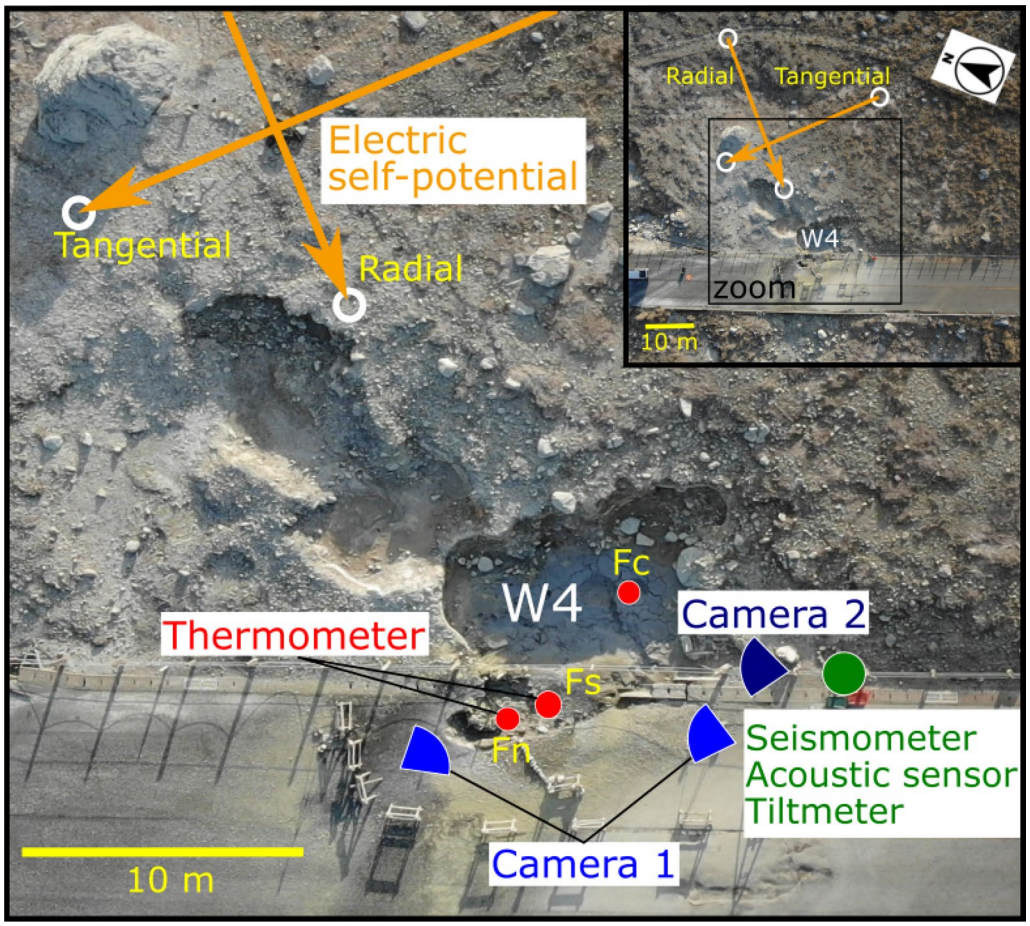

Fig. 2 Annotated drone photograph of the layout of observational equipment in and around crater W4. Red circles in the figure indicate the locations of the three vents (Fn, Fs, and Fc). White circles indicate the locations of the four self-potential electrodes

the crater in 2018. In August 2020, the temperature of the fumarole increased, and new vents were formed near W4 (Tajima et al. 2021). Images captured from a Japan Meteorological Agency (JMA) monitoring camera during March 2021 showed that the fumarole of W4 often disappeared (Matsushima et al. 2021).

We performed multi-parametric observations from 20 April to 4 May 2021 and identified intermittent hydrothermal water discharge. The details of observations are described in following section. During the period when the intermittent hydrothermal water discharge occurred, three vents were identified inside W4, vents Fs, Fn, and Fc (Fig. 2), each with a diameter of approximately 10 cm. Vent Fn is positioned approximately 30 cm higher than vent Fs (Additional file 5: Fig. S1). A single cycle of hydrothermal water discharge and evacuation lasts for 14–70 h (see below section). These times are longer than those of typical geysers in the world. Similar intermittent long-duration hydrothermal water discharge phenomena have been reported from crater lakes. At Shinyu Hot Spring in Japan, the duration of spouting is approximately 10 days (Fukui et al. 2020). At Inferno Crater Lake in New Zealand, the water level fluctuates over a period of 40 days (Scott 1994). Ruapehu Crater Lake in New Zealand has also shown cyclic heating and cooling with a period ranging from 6 to 12 + months (Vandemeulebrouck et al. 2005). At West Crater, after the study period involving multi-parametric observations, we continued to collect temperature and visual (camera) data and we confirmed the discharge activity terminated on 2 July 2021. After 2 July, there was no more hydrothermal water discharge or steam effusion at West Crater. In addition, we observed a drastic change in discharge style (including interval) on 4 June 2021, two weeks before the complete cessation of discharge activity. Change in discharge style is discussed below in below section.

Table 1 Summary of data acquisition during 2021

Observation	Sensor	Observation frequency	Duration
Camera 1	TLC200 Pro (Brino)	1 min	20 April to 4 May
Camera 2	Radiant40	2 min	4 May to 20 September
Temperature	RTR505BPt100 (T&D)	1 min	20 April to 20 September
Electric self-potential	Non-polarized (Pb-PbCl) electrodes	32 Hz	20 April to 4 May
Ground motion (seismicity)	LE-3D/lite (Lennartz Electronic)	200 Hz	20 April to 4 May
Acoustics	SI104 (Hakusan)	200 Hz	20 April to 4 May
Tilt	701-2A (Jewell)	100 Hz	20 April to 4 May

Observations

Visual camera

Figure 2 and Table 1 present the locations of observational instruments and a summary of data acquisition, respectively. Movies were recorded by time-lapse cameras (Brinno TLC200Pro) with an interval of 1 min from 20 April to 4 May. Two cameras ("Camera 1" in Fig. 2 and Table 1) were set to focus on vents Fn and Fs, respectively. Visual imaging was unable to be performed during night-time (19:00–05:00). Recording was stopped at 19:30 on 1 May for vent Fs and at 00:32 on 3 May for vent Fn. We used movie image data mainly from vent Fs, as the camera for this vent captured the activity more clearly than that for vent Fn. After 4 May, we installed an infrared camera (Radiant40; "Camera 2" in Fig. 2 and Table 1) with an interval of 2 min until 20 September 2021 to monitor vent Fs during night-time.

Thermometer

Pt100 resistance thermometers were installed at the heads of vents Fs and Fn. Temperature was recorded using a sampling frequency of 1 min from 20 April to 20 September 2021. The elevation of West Crater is 1233 m, and the boiling point of pure water at this elevation is approximately 96 °C.

Electric self-potential (SP)

Using non-polarizable electrodes (Pb–PbCl), wires, and an electric field logger (NT system design ELOG1K), the naturally occurring voltage difference (in mV) was recorded along two directions (radial and tangential to the vent Fs; Fig. 2) at a sampling frequency of 32 Hz. The voltage in two independent dipoles (30 m length, radial and tangential directions) was measured. In this study, we used 1 Hz down-sampled time-series data with arithmetic averaging.

Seismometer

A seismometer (Lennartz LE3D-lite, eigenfrequency of 1 s) was installed 8 m south of the vent Fs (Fig. 2). Three components [vertical or up–down (U–D), N–S, and E–W] of ground velocity data (μm/s) were recorded at a sampling frequency of 200 Hz.

Acoustic sensor

Acoustic signals were recorded using a Hakusan SI104 microphone, which has a flat response in the 0.05–1500 Hz range. The sensor was installed 8 m south of the vent Fs (Fig. 2), and acoustic waves (Pa) were recorded at a sampling frequency of 200 Hz. Time-series data of the seismometer and acoustic sensor were recorded using an HKS-9700 logger (Keisokugiken Corp.).

Tiltmeter

We installed a tiltmeter (Jewell 701-2A) in a hole of 30 cm depth, 8 m south of the vent Fs. The sampling frequency was 100 Hz. Time-series data for ground tilt (μ-radian) were recorded by an LS8800 logger (Hakusan Corp.). We recorded the E–W and N–S components. Equipment outage caused a period of missing data from 17:27 on 22 April to 11:39 on 24 April.

Data

Camera (movie) data

Additional file 1: Movie S1 and Additional file 2: Movie S2 show examples of intermittent hydrothermal water discharge at W4. On the basis of the movie data for vent Fs, we divided the eruption cycle into four phases as follows: (i) cessation of steam effusion; (ii) onset of hydrothermal water discharge; (iii) active steam effusion; and (iv) drainback of the hydrothermal water pool at vent Fs. Here, we explain each phase on the basis of visual camera observations. (i) Effusion of steam from vents Fs and Fn stopped approximately 20–40 min before the onset of hydrothermal water discharge (Fig. 3b; Additional file 1: Movie S1 and Additional file 3: Movie S3). (ii) Hydrothermal water discharge started slowly without steam from vent Fs. Discharged water flowed into two parts: inflow into W4 and accumulation at vent Fs, which together formed a hydrothermal water pool (Fig. 3b; Additional file 1: Movie S1

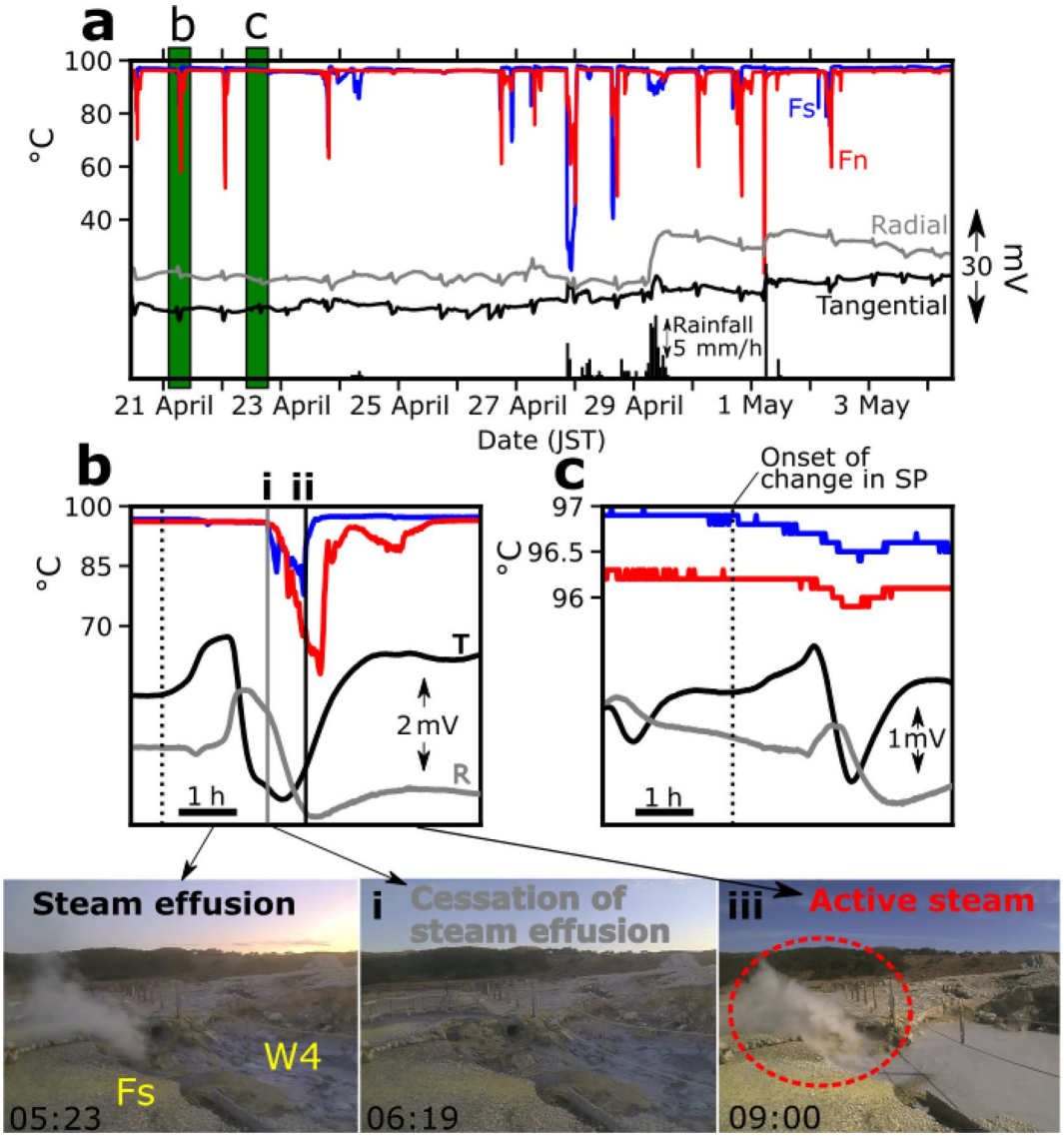

Fig. 3 Temporal variations in temperature and electric self-potential (SP) associated with intermittent hydrothermal water discharge. **a** Temperature of Fs and Fn, tangential (T) and radial (R) SP signals, and rainfall data for the period 20 April to 4 May 2021. Rainfall data were obtained from the Ebino site (Fig. 1). **b** Data for temperature and SP for the period 04:00 to 10:00 on 21 April (JST), with snapshots from the movie data. The timings of onset of change in SP (dotted line), cessation of steam discharge (gray line labeled "i"), onset of hydrothermal water discharge (black line labeled "ii") and active steam effusion (photograph "iii") are shown. The onset time of change in SP was determined from the tangential component. **c** Data for temperature and SP data for the period 13:30 to 17:30 on 22 April 2021 (JST)

and Additional file 3: Movie S3). (iii) Steam effusion at vents Fs and Fn gradually became active, and hot water in the pool of vent Fs gradually decreased (Additional file 2: Movie S2). (iv) Approximately 1–1.5 h before the next hydrothermal water discharge, drain-back of the hydrothermal water pool occurred at vent Fs (Additional file 2: Movie S2). The small water pool at vent Fs in some instances dried up before the timing of drain-back, in which case, drain-back of hydrothermal water could not be visually confirmed (Fig. 3).

Temperature data

Figure 3 shows the variation in temperature and SP during the period of multi-parametric observations. During strong steam effusion, the temperatures of vents Fs and Fn were maintained at ~ 96 ℃, which is the boiling point at this elevation (1233 m; Fig. 3). The temperature decreased at both vents when steam effusion stopped. Approximately 20–40 min after the cessation of steam effusion, hydrothermal water discharge started, and the temperature at vent Fs increased rapidly (Fig. 3b). When

hydrothermal water discharge began, the temperature was 80–90 ℃ but increased to 96 ℃ 7–14 min later. The temperature at vent Fn started to increase approximately 12–20 min later than that at vent Fs, probably because the position of vent Fn was approximately 30 cm higher relative to vent Fs (Additional file 5: Fig. S1), and thus the upwelling hydrothermal water filled vent Fn later than Fs.

Electric self-potential (SP) data

SP shows clear cyclic change (Fig. 3). Figure 3b exhibits a typical pattern of SP temporal change associated with surface hydrothermal water discharge, whereas Fig. 3c shows the pattern without surface hydrothermal water discharge. In the latter case, SP shows clear temporal change and is accompanied by a small change in temperature (0.2–0.9 ℃). At the time of initiation of the change in SP, we did not observe any corresponding changes at the ground surface. For events with hydrothermal water discharge, the temporal change in SP starts approximately 2 h before the onset of hydrothermal water discharge (Fig. 3b). For events without hydrothermal water discharge, the temporal change in SP starts 1 to 3 h before a slight temperature rise (Fig. 3c). It should be noted that there was no fumarolic zone or hydrothermal water discharge at the locations of four (two radial, two tangential) electrodes (Fig. 2). Therefore, a thermoelectric effect can be excluded as a cause of variation in SP. Previous studies in New Zealand of Iodine geyser with an average cycle of 160–180 s and Pohutu geyser with a cycle of several minutes have shown that cyclic SP change can be associated with geyser eruptions (Nishi et al. 2000; Legaz et al. 2009a). The temporal change in SP at geysers has been explained by an electrokinetic mechanism involving groundwater movement through porous material (e.g., Mizutani et al. 1976; Ishido and Mizutani 1981). In a typical rock–water system, the downstream direction shows positive voltage (i.e., a positive SP zone represents the region to which groundwater flows). However, it has been suggested that variation in SP is controlled by the pH of porewater in the geyser field (Legaz et al. 2009a). The relationship between pH and variation in SP is discussed in following section. In this study, we similarly interpret a change in SP as being generated by subsurface groundwater flow. It is noted that the electrokinetic mechanism depends on the electric charge separation in an electrical double layer whose thickness is in the order of nanometers (e.g., Ishido and Mizutani 1981; Revil et al. 1999). The surface area of the solid–water interface governs the amount of electric charge. Therefore, SP cannot be generated by groundwater flow in a pipe-like conduit or fractures owing to the insufficient electric charge in such structures but can be generated by groundwater flow in porous material. This is an important aspect to consider with respect to identifying the mechanism of intermittent hydrothermal water discharge.

A temporal change in electrical resistivity structure may partly contribute to a temporal change in SP. This possible influence has been indicated by theoretical work (Ishido and Pritchet 1999; Revil and Jardani 2013) and numerical simulations (Ishido 2004; Byrdina et al. 2013). Temporal change in resistivity beneath West Crater needs to be investigated in the future using time-lapse resistivity surveys. Legaz et al. (2009b) observed a change in resistivity structure synchronous with change in water level in Inferno Crater Lake, but did not observe any corresponding change in SP.

Seismic data

For seismic data, we divided signals into two frequency ranges: (A) signals in the frequency range of > 20 Hz, and (B) signals in the frequency range of < 20 Hz. Figure 4 shows an example of the multi-variable data for one cycle associated with the hydrothermal water discharge. Figure 5 shows multi-variable data for four cycles, all of which show hydrothermal water discharge. Signal (A) started to decrease when drain-back occurred ("iv" in Fig. 4), but signal (B) started to decrease prior to the occurrence of drain-back. Approximately 1 to 4 h after the onset of hydrothermal water discharge ("iii" in Fig. 4), signal (B) increased rapidly (Figs. 4 and 5). However, there was no corresponding change in signal (A). Given these differing patterns, seismic signals (A) and (B) are thought to have different tremor sources.

Acoustic data

For acoustic data, we focused on signals in the frequency range of > 20 Hz because infrasound (< 20 Hz) is highly affected by wind. The acoustic signals decreased when drain-back occurred ("iv" in Fig. 4). After the onset of hydrothermal water discharge, the signals gradually increased ("ii" in Fig. 4). Approximately 1 to 4 h later, the signals increased more dramatically ("iii" in Figs. 4 and 5). We interpret that the acoustic signals with a frequency of > 20 Hz were generated from surface activity, such as splashing of the water surface of the hydrothermal pool at vent Fs. The acoustic signals and seismic signals with a frequency of > 20 Hz may have the same origin, as changes in both signal types occurred simultaneously ("iii" in Fig. 4).

Tilt data

Change in tilt associated with hydrothermal water discharge was identified from the measured tilt data. Because tilt data are strongly affected by long-term fluctuations (e.g., rainfall and temperature), we calculated the moving average using a 4-h window and

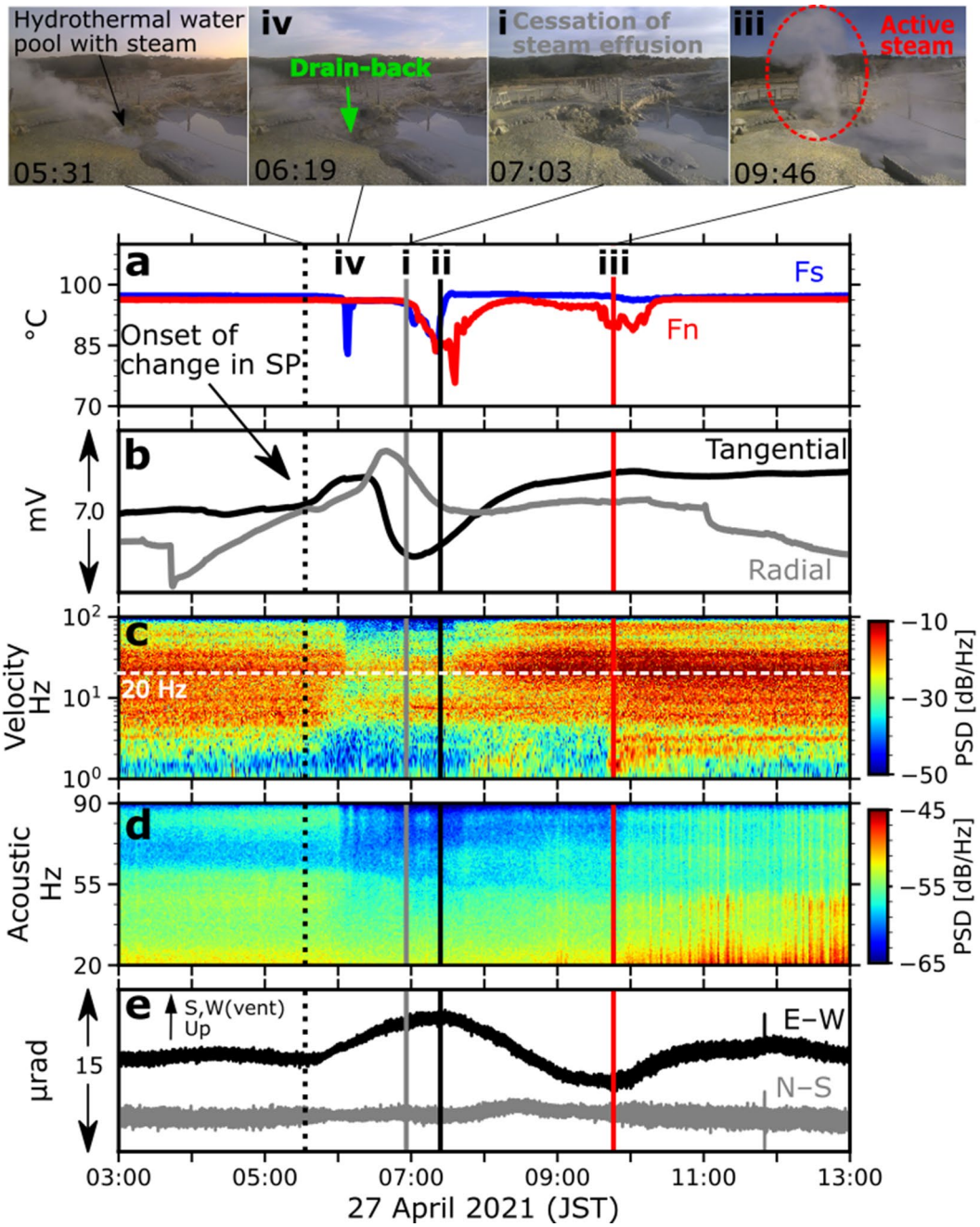

Fig. 4 Example of multi-observational data during a hydrothermal water discharge event [03:00 to 15:00 on 27 April 2021 (JST)]. The snapshots are from Camera 1 of vent Fs. The times of the photographs correspond to those in the time-series graph. **a** Temperature, **b** electric self-potential, **c** spectrogram of the seismic signal (up–down component), **d** spectrogram of the acoustic signal, and **e** tilt. Power spectral density (PSD; dB/Hz) is $(\mu m/s)^2$/Hz for panel **c** and $(Pa)^2$/Hz for panel **d**. The presented time series are part of Additional file 5: Fig. S1 and Additional file 1: Movie S1. The timings of onset of change in SP (dotted line), cessation of steam discharge (gray line labeled "i"), onset of hydrothermal water discharge (black line labeled "ii"), onset of active steam discharge (red line labeled "iii"), and onset of drain-back (photograph "iv") are shown

subtracted it from the raw data to detrend long-term fluctuations. The use of shorter time windows yields similar results (Additional file 5: Fig. S2). Figure 4 shows that E–W tilt (i.e., uplift in the direction toward the vent Fs) started to increase around the time of onset of change in SP. When hydrothermal water discharge occurred, the E–W tilt showed subsidence in the direction toward the vent ("ii" in Fig. 4). When

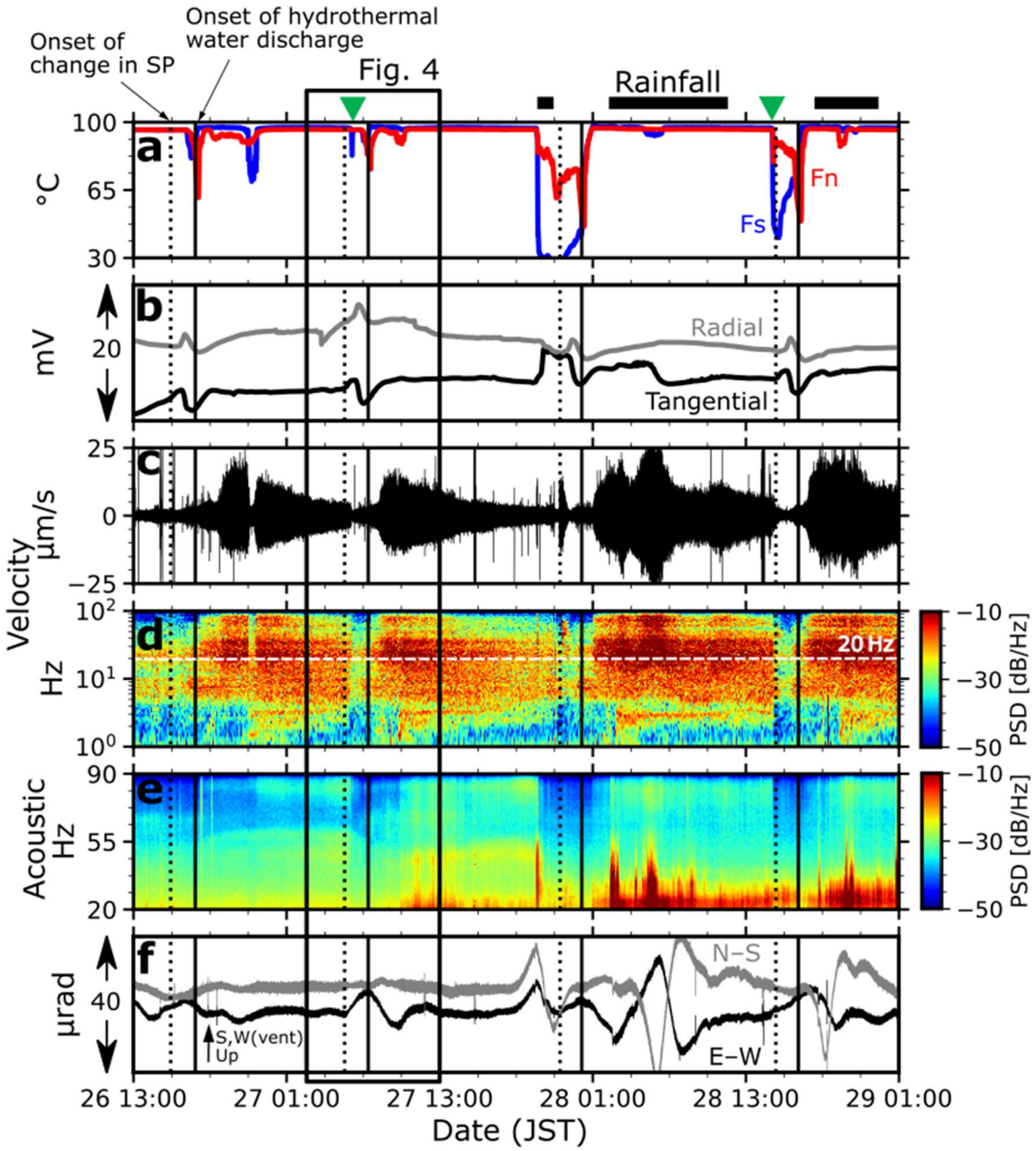

Fig. 5 Temporal variations in **a** temperature, **b** electric self-potential, **c** non-filtered seismic signal (up–down component), **d** spectrogram of the seismic signal, **e** spectrogram of the acoustic signal, and **f** tilt for the period from 13:00 on 26 April to 01:00 on 29 April (JST). The timings of onset of change in SP and onset of hydrothermal water discharge are indicated by dotted and black lines, respectively. We judged the timing of hydrothermal water discharge on the basis of images from Camera 1 and temperature data for vent Fs. The timing of rainfall and drain-back are indicated by black lines and green inverted triangle at the top of the figure, respectively

the seismic signals increased rapidly ("iii" in Fig. 4), the change in E–W tilt stopped. It is noted that such correlation is found in other cycles, but temporal change also occurred when no geophysical change was observed (Fig. 5 and Additional file 5: Fig. S3). Because the cycle of the hydrothermal water discharge was long, in the range of 14–70 h, the tilt data may have been affected by unknown noise.

Data after the period of multi-parametric observations

After the period of multi-parametric observations (20 April to 4 May 2021), we continued camera and

temperature observations, which overall covered the period 20 April to 20 September 2021 (Table 1). This period of extended observations captured a significant change in the style of hydrothermal water discharge. Figure 6 shows temperature data measured at vents Fs and Fn, rainfall data recorded at the Ebino observation site (JMA; Fig. 2), and the timing of hydrothermal water discharge. On the basis of these data, we defined three discharge styles, as follows.

Style 1 (Additional file 2: Movie S2) involved hydrothermal water discharge from vent Fs and steam effusion from vent Fn. This style was observed during the period of multi-parametric observations (Fig. 3). The discharge interval was approximately 14–70 h. This style was mainly identified as occurring until 11 May 2021.

Style 2 (Additional file 3: Movie S3) was observed after heavy rain from 14 to 22 May and involved hydrothermal water discharge simultaneously from vents Fs and Fc from 22 May to 6 June. The discharge interval was approximately 18–40 h.

Style 3 (Additional file 4: Movie S4) was observed from 4 to 28 June. The upper panel in Fig. 6 shows the change in temperature and the timing of hydrothermal water discharge, revealing repeated hydrothermal water discharges from vent Fs with an interval of 1–2 h multiple times in a row. After multiple hydrothermal water discharges, steam effusion continued for a few hours until the next multiple hydrothermal water discharges occurred.

Discussion

Inflow of groundwater

The amplitude of SP was observed to increase before hydrothermal discharge (Fig. 3). To clarify the temporal relationship between SP and hydrothermal water discharge, we examined the temporal variation in SP amplitude for events with hydrothermal water discharge (Fig. 7a). The reference is the value of SP when the SP tangential components start to change (dotted lines in Figs. 3 and 5). The temporal variations in SP for each event (gray in Fig. 7a) and in the arithmetic mean of all events (colored) show that steam effusion ceased when SP amplitude reached its peak and that hydrothermal water discharge occurred when SP amplitude started to decrease. It is noted that the phreatic explosion during the 2018 eruption of Iwo-Yama occurred when the SP amplitude measured at a distance of 500 m from the eruption vent started to decrease (Aizawa et al. 2022). The analogy between hydrothermal water discharge and phreatic explosion is discussed below in following section.

We calculated SP particle motion (Fig. 7c and d) by assuming that the dipole length (length between electrodes) is smaller than the spatial scale of regional SP change. As only one SP measurement site was employed in this study, we were unable to judge the validity of this assumption. However, particle motion may provide qualitative information about the direction of groundwater flow (Aniya et al. 2022). The SP particle motion showed a gradual increase in the radial component (i.e., SP increased at the electrode near the vent Fs) before the cessation of steam effusion (Fig. 7c). This suggests that groundwater flow toward the region underlying the vent Fs occurred before hydrothermal water discharge. Compared with the events without hydrothermal water discharge (Fig. 7d), the SP radial component of events with hydrothermal water discharge is larger, which suggests that the flow of groundwater toward the region underlying the vent Fs contributed to the preparatory process of hydrothermal water discharge. In addition, the SP radial component was approximately zero at the onset of hydrothermal water discharge. This suggests that the groundwater flow toward the region underlying the vent Fs decreased at the time of hydrothermal water discharge. We note here that the SP tangential component was measurable at the time of hydrothermal water discharge, on which basis we interpret that there was some tangential groundwater flow toward the region underlying the vent Fs at the time of hydrothermal water discharge. In accordance with the SP data, the uplift and subsidence of vent Fs in the tilt data (Fig. 4e and Additional file 5: Fig. S3) are interpreted as corresponding to the accumulation and discharge of groundwater, respectively. However, this interpretation regarding groundwater flow away from the SP sensor site is limited because of the single site employed and the locations of the electrodes.

In this study, we assumed a typical rock–water system (with negative zeta potential) that shows a positive voltage in the downstream direction. However, as the pH of the groundwater decreases, the zeta potential approaches zero, and its polarity can be positive (Ishido and Mizutani 1981; Revil et al. 1999; Aizawa et al. 2008; Leroy et al. 2008). In fact, the pH of the hydrothermal water pool in W4 is 1.00–1.43 (Ishibashi et al. 2021), suggesting that the downstream direction may show a negative voltage. In such a case, our interpretation of groundwater inflow would not be applicable. However, we infer on the basis of our multi-parametric observational data that the pH of cold groundwater is not as low as that observed on the hydrothermal water pool, and that groundwater inflow to the vent causes a change in SP before the discharge of hydrothermal water. Our inflow interpretation is consistent with the tilt data, which show uplift of the

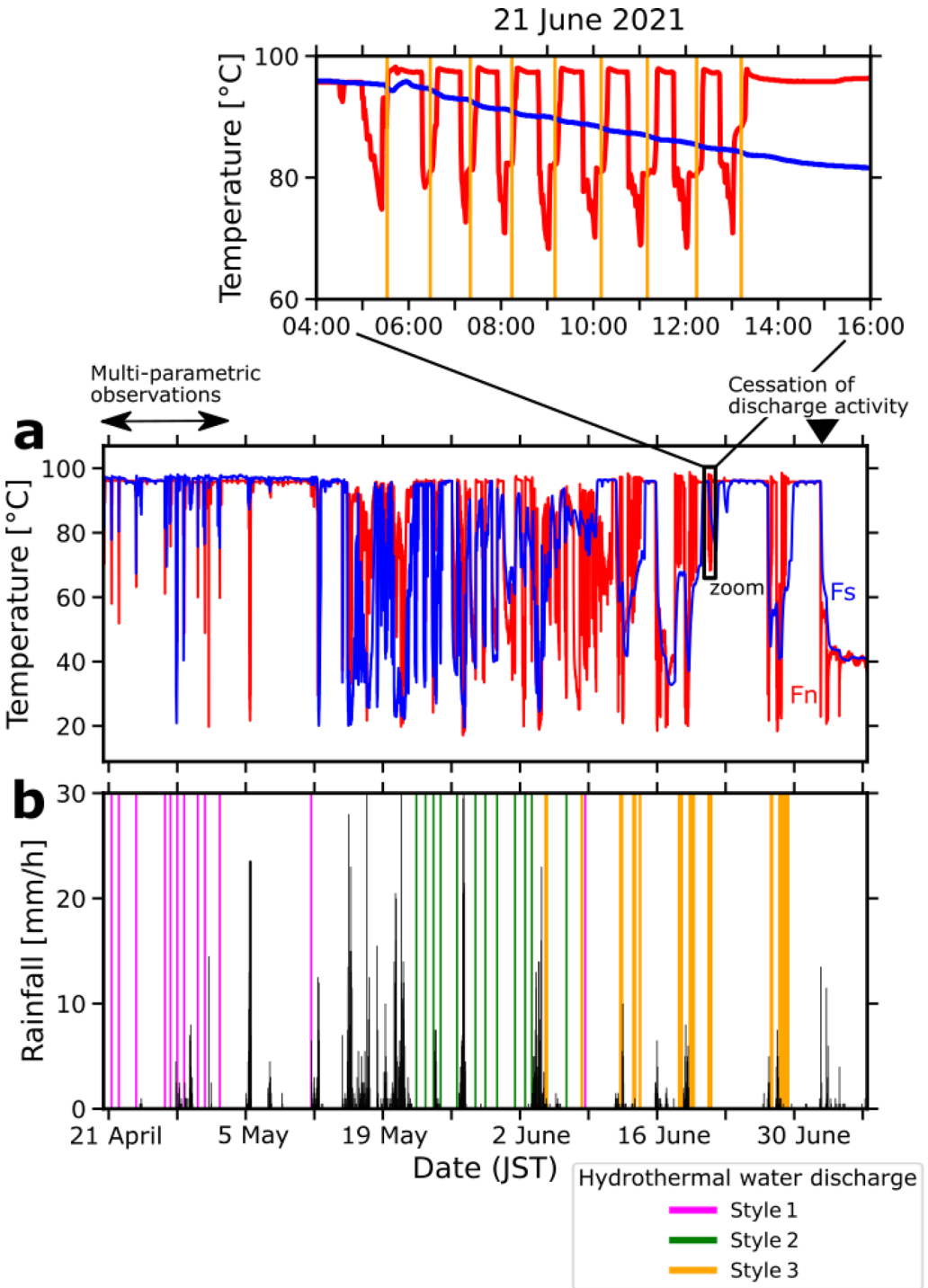

Fig. 6 Temporal variations in **a** long-term temperature and **b** rainfall for the period 20 April to 10 July. The period of multi-method observations was from 20 April to 4 May (Fig. 3). Rainfall data were obtained from the Ebino site (Fig. 1). Purple, green, and orange vertical lines in the upper and lower panels represent the timings of hydrothermal water discharge judged from the visual movie. We judged the timing of hydrothermal water discharge on the basis of images from cameras 1 and 2 (Fig. 2 and Table 1)

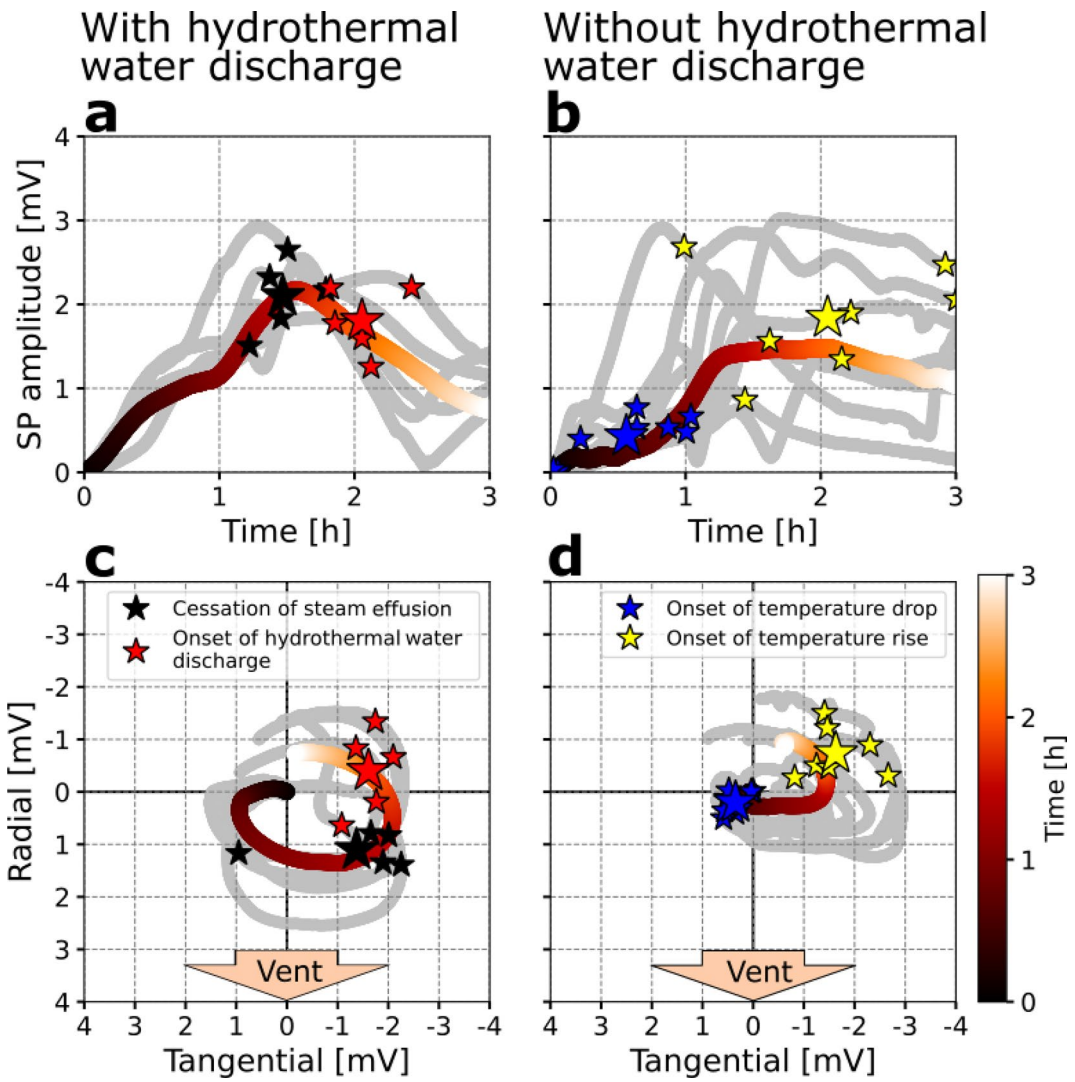

Fig. 7 Temporal variation in electric self-potential (SP). **a** Temporal change in the amplitude of SP associated with hydrothermal water discharge, using data only from those events for which the occurrence of hydrothermal water discharge was confirmed by visual camera images. Gray lines correspond to events, and the colored line represents the average of all events. Black and red stars correspond to the timings of the cessation of steam effusion and the onset of hydrothermal water discharge, respectively (large stars show their averages). **b** Temporal change in the amplitude of SP without hydrothermal water discharge. Blue and yellow stars correspond to the timings of temperature rise and fall at vent Fs, respectively. **c** Particle motions of change in SP with the occurrence of hydrothermal water discharge. Note that the dipole lengths of the radial and tangential directions are the same (30 m). **d** Particle motions of change in SP without the occurrence of hydrothermal water discharge

vent before hydrothermal water discharge. We infer that the low pH of the hydrothermal water pool is caused by mixing of deep volcanic volatiles and cold, near-surface groundwater.

Mechanism of intermittent hydrothermal water discharge

Plumbing system

Here, we discuss the mechanism of the observed intermittent hydrothermal water discharge. First, we need to assume the underground plumbing system, as inferred on the basis of broad observational constraints. Geysers form and are active in regions with sufficient water supply and a source of heat (Hurwitz and Manga 2017). Iwo-Yama is located in an active geothermal field that has been in operation since around AD1900 and underwent a small phreatic eruption in April 2018 (Tajima et al. 2020). Therefore, Iwo-Yama has sufficient groundwater and heat source to generate hydrothermal/geyser activity. In addition, geological features such as landslide deposits favor the formation of multiple complex systems of subterranean conduits and cavities (Belousov et al. 2013). The surface of Iwo-Yama is covered by debris avalanche

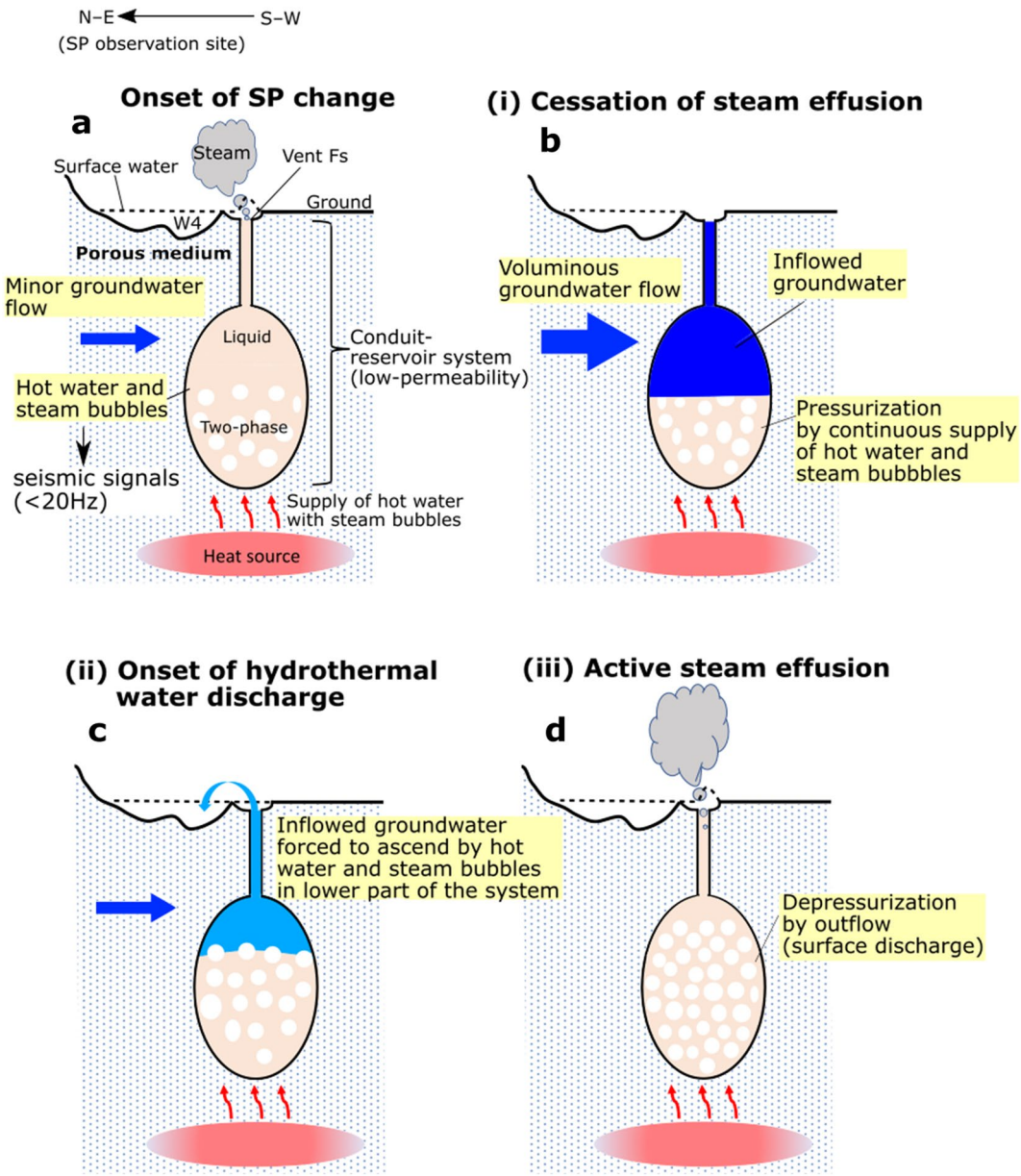

Fig. 8 Schematic model of intermittent hydrothermal water discharge. Red and blue colors represent high and low temperatures, respectively. **a** Onset of change in SP, **b** cessation of steam effusion, **c** onset of hydrothermal water discharge, and **d** active steam effusion. Numerals "i" to "iii" in the panel titles correspond to those referred to in the main text

deposits generated by the 4.3 ka phreatic eruption of Karakuni-dake (Fig. 1; Tajima et al. 2014), which may have favored the generation of a system of complicated conduits and reservoir (s). For examining the cycle of the intermittent hydrothermal water discharge, we assumed a simple plumbing system that consists of a vertical conduit and a cavity that acts as a hydrothermal water reservoir (conduit–reservoir system). A vertical conduit and cavity may constitute a low-permeability fracture network inside the conduit–reservoir system (Ingebritsen and Rojstaczer 1993; Vandemeulebrouck et al. 2005).

Preparatory process of hydrothermal water discharge

Approximately 2 h before hydrothermal water discharge, groundwater started to flow toward the region underlying the vents (Fig. 8a), consistent with the temporal change in SP (Fig. 7) and the surface uplift toward the vents (Fig. 4e and Additional file 5: Fig. S3). The triggering mechanism

of groundwater inflow is unclear and difficult to investigate. One possible mechanism is gravitational instability in the conduit–reservoir system (Vandemeulebrouck et al. 2005; Legaz et al. 2009b). When a liquid-dominated layer exists over a two-phase layer (Fig. 8a), gravitational instability or convection may occur, which may trigger an inflow of cold groundwater from the surrounding region. Vandemeulebrouck et al. (2005) proposed that changes in water level in Inferno Crater Lake are due to fluid phase changes in the heat pipe caused by gravitational instability or convection.

At the onset of change in SP, seismic signals with a frequency of < 20 Hz were recorded but started to decrease 15–45 min after the onset of change in SP (Fig. 4c). We interpret that the seismic signal was generated by bubble activity (growing, collapsing or moving) in boiling fluid (e.g., Kieffer 1984; Vandemeulebrouck et al. 2013; Gresse et al. 2018; Wu et al. 2019). Boiling can be inhibited by the inflow of cold water (Namiki et al. 2016), and we infer that in the case of the vents at W4 of Iwo-Yama, inflow of cold water inhibited water boiling in the conduit–reservoir system. A part of hydrothermal water can be replaced by inflowed cold water. This might have caused temporary discharge of hydrothermal water at depth, which is visually observed as drain-back of hydrothermal water from the pool in W4. SP data suggest that the inflow of cold groundwater gradually increased until the cessation of steam effusion (Fig. 7a). Therefore, we interpret that a large volume of groundwater flowed into the conduit–reservoir system and accumulated above the hot water within the lower part of the system (Fig. 8b). This may explain the cessation of steam effusion approximately 20–40 min before the onset of hydrothermal water discharge.

Onset of hydrothermal water discharge

SP data suggest that before hydrothermal water discharge, the inflow of cold groundwater gradually decreased (Fig. 7a), and seismic signals with a frequency of < 20 Hz increased after the cessation of steam effusion (phases "i" to "ii" in Fig. 4). We interpret that pressurization sufficient to force the water in the upper part of the conduit–reservoir system to ascend might have occurred in the lower part of the system owing to the decrease in the volume of inflowed groundwater in the upper part of the system and the continuing supply of steam bubbles and hot water (Fig. 8c). This interpretation is supported by the low temperature of the initially discharged water (80–90 ℃). Seismic signals with a frequency of < 20 Hz may have increased owing to the re-initiation of bubble growth after the cessation of steam effusion.

Active steam effusion

One to four hours after hydrothermal water discharge occurred, seismic signals with a frequency of < 20 Hz and acoustic signals with a frequency of > 20 Hz increased ("iii" in Fig. 4). These signals suggest an increase in the amount of boiling in the conduit–reservoir system and corresponding steam effusion from the vent Fs (Fig. 8d). We infer that after the onset of hydrothermal water discharge, depressurization of the conduit–reservoir system occurred as a result of hydrothermal water outflow from the upper part of the system, which promoted boiling in the system (Fig. 8d).

Similarity of the geyser eruption system to volcanic eruptions

Inflow (influx) of cold groundwater has also been suggested as a contributing mechanism to the 2018 phreatic eruption of Iwo-Yama. Aizawa et al. (2022) measured a series of 13 temporal changes (events) in tilt, tremor, and horizontal electric field near the Iwo-Yama eruption vent. One of these events occurred immediately before the onset of the 2018 phreatic eruption. Those authors interpreted that a potential phreatic eruption was inhibited by flow of near-surface, cold groundwater toward the region underlying the active vent but that an explosive phreatic eruption occurred when the intrusion of hot water was shallow and groundwater flow was limited. Therefore, the presence and flow of near-surface groundwater is likely a key control on the occurrence of phreatic eruptions. In this study, we suggest that the inflow of cold groundwater into the conduit–reservoir system is also a key control on the observed cyclic hydrothermal water discharge. Our results suggest that electric field measurements as used at geyser sites may be useful for the study of volcanic eruptions.

Change in discharge style

We identified a change in discharge style over time from style 1 to style 2 to style 3 at vents in W4 (Fig. 6). It is known that the interval between geyser eruptions depends on a delicate balance between underground processes, such as the supply of heat and water (Wendel 2014). Geyser activity can change according to variations in precipitation and climate, which influence the supply of groundwater that feeds the eruptions (Hurwitz et al. 2008, 2021).

In the previous section, we proposed that the inflow of cold groundwater into the conduit–reservoir system controlled the cyclic occurrence of hydrothermal water discharge. Discharge style 2 (green in Fig. 6b) took place after high precipitation during mid-May, and style

3 (orange in Fig. 6b) took place after high precipitation during early June. The change in discharge style from style 1 to style 2 and style 2 to style 3 is thus inferred to be related to the occurrence of high precipitation. Tsukamoto et al. (2018) described a low-permeability, clay-rich layer at depths of 200–700 m below the surface of Iwo-Yama, with this clay-rich layer being overlain by a groundwater-dominated layer. High precipitation may have increased the amount of water in this groundwater layer; therefore, the volume of inflow of groundwater into the conduit–reservoir system (Fig. 8b) may have increased as a result of the high precipitation and may in turn have caused the change in discharge style.

Conclusion

We investigated intermittent hydrothermal water discharge at Iwo-Yama West Crater during April–July 2021. During the period of multi-parametric observations (20 April to 4 May), the cycle of the discharge lasted for 14–70 h, and the course of a single cycle followed this sequence of phases: (i) cessation of steam effusion; (ii) onset of hydrothermal water discharge; (iii) active steam effusion; and (iv) drain-back (evacuation) of water from the hydrothermal water pool at vent Fs. However, the discharge style and cycle changed after the period of multi-parametric observations. The change in discharge style and cycle coincided with periods of high precipitation, suggesting that an increase in the volume of inflow of groundwater into the conduit–reservoir system caused by the high precipitation may have led to the change in discharge style.

Observational data (movie, temperature, SP, seismic, acoustic, and tilt) showed changes corresponding to the phases of the cycle of intermittent hydrothermal water discharge. In particular, change in SP generated by groundwater flow started approximately 2 h before the onset of hydrothermal water discharge and SP increased until the cessation of steam effusion. We interpret that the inflow of cold groundwater inhibited the boiling of water in the hydrothermal plumbing system and thereby caused steam effusion to cease. SP data also suggest that the inflow of cold groundwater subsequently gradually decreased, allowing a corresponding increase in pressure to occur in the lower part of the conduit–reservoir system as a result of the decrease in the volume of inflowed groundwater in the upper part of the system and the continuing supply of steam bubbles and hot water. Boiling of the underlying hot water finally caused the groundwater in the upper part of the conduit–reservoir system to ascend, generating hydrothermal discharge. Overall, the results of our study show that cyclic hydrothermal water discharge into West Crater of Iwo-Yama volcano was controlled by the inflow of cold groundwater into the conduit–reservoir system.

Abbreviations

JMA	Japan Meteorological Agency
JST	Japan Standard Time
KVC	Kirishima Volcanic Complex
SP	Electric self-potential

Supplementary Information

The online version contains supplementary material available at https://doi.org/10.1186/s40623-023-01830-7.

Additional file 1: Movie S1. Movie data from Camera 1 at vent Fs for 21 April 2021.

Additional file 2: Movie S2. Movie data from Camera 1 at vent Fs for 27 April 2021.

Additional file 3: Movie S3. Movie data from Camera 2 for 22 May 2021.

Additional file 4: Movie S4. Movie data from Camera 2 for 21 June 2021.

Additional file 5: Fig. S1. Photograph showing the locations of vents Fn and Fs, taken on 20 September 2021. Fig. S2. Raw time-series of tilt data for the period from 13:00 on 26 April to 01:00 on 29 April.Detrended long-term fluctuations obtained by removing the moving average calculated using time windows of 1, 2, 3, and 4 h, respectively. The timings of onset of change in SP and onset of hydrothermal water discharge are indicated by dotted and black lines, respectively. Fig. S3. Time-series tilt data for six different 12 h periods. Panels a to f show different events. The dotted line in each case represents the onset time of change in SP [a 04:52 on 21 April, b 23:06 on 21 April, c 15:55 on 26 April, d 05:33 on 27 April, e 22:26 on 27 April, and f 15:21 on 28 April]. Black, red, and green stars correspond to the timings of the cessation of steam effusion, onset of hydrothermal discharge, and increase in the strength of the seismic signal, respectively. The events shown in panels b and f do not have black or red stars because the periods extended through night-time hours.

Acknowledgements

We thank S. Aniya, K. Yoshinaga, and T. Watanabe for providing support and arrangements for the field survey. Constructive comments from Jean Vandemeulebrouck and Marceau Gresse greatly improved the manuscript. This work was supported by the Ministry of Education, Culture, Sports, Science and Technology (MEXT) of Japan, under the Integrated Program for Next Generation Volcano Research and Human Resource Development (grant number JPJ005391).

Author contributions

HT analyzed the data. HT and KA drafted the manuscript. TM, DM, and HT contributed to data acquisition and maintaining the observation network. KA supported the analysis and developed the theoretical background. All authors read and approved the final manuscript.

Funding

This work was supported by the Ministry of Education, Culture, Sports, Science and Technology (MEXT) of Japan, under the Integrated Program for Next Generation Volcano Research and Human Resource Development (Grant number JPJ005391).

Availability of data and materials

Data are available at the JVDN site with registration using a free account (https://jvdn.bosai.go.jp/app/pages/index.html?root=anyFileEdit&id=da15eb71-e866-4a29-ac90-463c20aaf1e6) or for download at the SEVO site (http://www.sevo.kyushu-u.ac.jp/open_file/Tanabe_et_al_2023.zip).

Declarations

Ethics approval and consent to participate
Not applicable.

Consent for publication
Not applicable.

Competing interests
The authors declare that they have no competing interests.

Author details
[1]Department of Earth and Planetary Sciences, Graduate School of Science, Kyushu University, 744 Motooka, Fukuoka 819-0395, Japan. [2]Institute of Seismology and Volcanology, Faculty of Science, Kyushu University, Shinyama 2, Shimabara 855-0843, Japan. [3]Earthquake Research Institute, University of Tokyo, Yayoi 1-1-1, Bunkyo-ku, Tokyo 113-0032, Japan.

Received: 8 October 2022 Accepted: 22 April 2023
Published online: 11 May 2023

References

Adelstein E, Tran A, Munoz-Saez C, Shteinberg A, Manga M (2014) Geyser preplay and eruption in a laboratory model with a bubble trap. J Volcanol Geotherm Res 285:129–135. https://doi.org/10.1016/j.jvolgeores.2014.08.005

Aizawa K, Uyeshima M, Nogami K (2008) Zeta potential estimation of volcanic rocks on 11 island arc-type volcanoes in Japan: implication for the generation of local self-potential anomalies. J Geophys Res Solid Earth 113:B02201. https://doi.org/10.1029/2007JB005058

Aizawa K, Ogawa Y, Ishido T (2009) Groundwater flow and hydrothermal systems within volcanic edifices: delineation by electric self-potential and magnetotellurics. J Geophys Res Solid Earth 114:B01208. https://doi.org/10.1029/2008JB005910

Aizawa K, Muramatsu D, Matsushima T, Koyama T, Uyeshima M, Nakao S (2022) Phreatic volcanic eruption preceded by observable shallow groundwater flow at Iwo-Yama, Kirishima Volcanic Complex, Japan. Commun Earth Environ 3:187. https://doi.org/10.1038/s43247-022-00515-5

Aniya S, Aizawa K, Matsushima T (2022) Infrasound–electric-field coupling associated with the 2018 Shinmoedake eruptions, Kirishima volcanic complex, Japan. Geophys Res Lett 49:e2021GL096555. https://doi.org/10.1029/2021GL096555

Belousov A, Belousova M, Nechayev A (2013) Video observations inside conduits of erupting geysers in Kamchatka, Russia, and their geological framework: implications for the geyser mechanism. Geology 41:387–390. https://doi.org/10.1130/G33366.1

Bryan TS (1995) The Geysers of Yellowstone, 3rd edn. University Press of Colorado, Denver

Bunsen R (1847) Physikalische Beobachtungen ueber die hauptsaechliche Geysir Islands. Poggendorffs Ann Phys Chem 72:159–170

Byrdina S, Ramos D, Vandemeulebrouck J, Masias P, Revil A, Finizola A, Gonzales Zuñiga K, Cruz V, Antayhua Y, Macedo O (2013) Influence of the regional topography on the remote emplacement of hydrothermal systems with examples of Ticsani and Ubinas volcanoes, Southern Peru. Earth Planet Sci Lett 365:152–164. https://doi.org/10.1016/j.epsl.2013.01.018

Cros E, Roux P, Vandemeulebrouck J, Kedar S (2011) Locating hydrothermal acoustic sources at Old Faithful Geyser using Matched Field Processing. Geophys J Int 187:385–393. https://doi.org/10.1111/j.1365-246X.2011.05147.x

Eibl EPS, Hainzl S, Vesely NIK, Walter TR, Jousset P, Hersir GP, Dahm T (2020) Eruption interval monitoring at Strokkur Geyser, Iceland. Geophys Res Lett 47:e2019GL085266. https://doi.org/10.1029/2019GL085266

Eibl EPS, Müeller D, Walter TR, Allahbakhshi M, Jousset P, Hersir GP, Dahm T (2021) Eruptive cycle and bubble trap of Strokkur geyser, Iceland. J Geophys Res Solid Earth 126:e2020JB020769. https://doi.org/10.1029/2020JB020769

Fukui K, Iida H, Kikukawa S (2020) Characteristics of water level change of the Shinyu Hot Spring Pond in Tateyama Caldera, converted to Geyser in 2014. J Hot Spring Sci 70:12–26 (**in Japanese with English abstract**)

Gresse M, Vandemeulebrouck J, Byrdina S, Chiodini G, Roux P, Rinaldi AP, Wathelet M, Ricci T, Letort J, Petrillo Z, Tuccimei P, Lucchetti C, Sciarra A (2018) Anatomy of a fumarolic system inferred from a multiphysics approach. Sci Rep 8:7580. https://doi.org/10.1038/s41598-018-25448-y

Hurwitz S, Manga M (2017) The fascinating and complex dynamics of geyser eruptions. Annu Rev Earth Planet Sci 45:31–59. https://doi.org/10.1146/annurev-earth-063016-015605

Hurwitz S, Kumar A, Taylor R, Heasler H (2008) Climate-induced variations of geyser periodicity in Yellowstone National Park, USA. Geology 36:451–454. https://doi.org/10.1130/G24723A.1

Hurwitz S, Sohn RA, Luttrell K, Manga M (2014) Triggering and modulation of geyser eruptions in Yellowstone National Park by earthquakes, earth tides, and weather. J Geophys Res Solid Earth 119:1718–1737. https://doi.org/10.1002/2013JB010803

Hurwitz S, Manga M, Campbell KA, Muñoz-Saez C, Eibl EPS (2021) Why study geysers? Eos 102. https://doi.org/10.1029/2021EO161365

Ingebritsen SE, Rojstaczer SA (1993) Controls on geyser periodicity. Science 262:889–892. https://doi.org/10.1126/science.262.5135.889

Ishibashi J, Masuda H, Mori K, Matsushima T (2021) Temporal variation of chemical composition of hot spring waters at Iwo-Yama West Crater. In: Report of 148th coordinating committee for prediction of volcanic eruption, JMA 1–2:40–43. (**in Japanese**) https://www.data.jma.go.jp/svd/vois/data/tokyo/STOCK/kaisetsu/CCPVE/shiryo/148/148_1-2.pdf

Ishido T (2004) Electrokinetic mechanism for the "W"-shaped self-potential profile on volcanoes. Geophys Res Lett 31:L15616. https://doi.org/10.1029/2004GL020409

Ishido T, Mizutani H (1981) Experimental and theoretical basis of electrokinetic phenomena in rock-water systems and its applications to geophysics. J Geophys Res 86:1763–1775. https://doi.org/10.1029/jb086ib03p01763

Ishido T, Pritchet JW (1999) Numerical simulation of electrokinetic potentials associated with subsurface fluid flow. J Geophys Res 104:15247–15259. https://doi.org/10.1029/1999JB900093

Johnson JB, Anderson JF, Anthony RE, Sciotto M (2013) Detecting geyser activity with infrasound. J Volcanol Geotherm Res 256:105–117. https://doi.org/10.1016/j.jvolgeores.2013.02.016

Kedar S, Sturtevant B, Kanamori H (1996) The origin of harmonic tremor at Old Faithful geyser. Nature 379:708–711. https://doi.org/10.1038/379708a0

Kedar S, Kanamori H, Sturtevant B (1998) Bubble collapse as the source of harmonic tremor at Old Faithful Geyser. J Geophys Res 103:24283–24299. https://doi.org/10.1029/98JB01824

Kieffer SW (1984) Seismicity at Old Faithful Geyser; an isolated source of geothermal noise and possible analogue of volcanic seismicity. J Volcanol Geotherm Res 22:59–95. https://doi.org/10.1016/0377-0273(84)90035-0

Kiryukhin AV, Karpov G (2020) A CO_2-driven gas lift mechanism in Geyser Cycling (Uzon Caldera, Kamchatka). Geosciences 10:180. https://doi.org/10.3390/geosciences10050180

Legaz A, Revil A, Roux P, Vandemeulebrouck J, Gouedard P, Hurst T, Boleve A (2009a) Self-potential and passive seismic monitoring of hydrothermal activity: a case study at Iodine Pool, Waimangu geothermal valley, New Zealand. J Volcanol Geotherm Res 179:11–18. https://doi.org/10.1016/j.jvolgeores.2008

Legaz A, Vandemeulebrouck J, Revil A, Kemna A, Hurst AW, Reeves R, Papasin R (2009b) A case study of resistivity and self-potential signatures of hydrothermal instabilities, Inferno Crater Lake, Waimangu, New Zealand. Geophys Res Lett 36:L12306. https://doi.org/10.1029/2009GL037573

Leroy P, Revil A, Kemna A, Cosenza P, Ghorbani A (2008) Complex conductivity of water-saturated packs of glass beads. J Colloid Interface Sci 321:103–117. https://doi.org/10.1016/j.jcis.2007.12.031

Lupi M, Collignon M, Fischanger F, Carrier A, Trippanera D, Pioli L (2022) Geysers, boiling groundwater and tectonics: the 3D subsurface resistive structure of the Haukadalur hydrothermal field, Iceland. J Geophys Res Solid Earth 127:e2022JB024040. https://doi.org/10.1029/2022JB024040

Mackenzie GS (1811) Travels in the Island of Iceland. Archibald Constable & Co, Edinburgh

Manga M, Brodsky E (2006) Seismic triggering of eruptions in the far field: volcanoes and geysers. Annu Rev Earth Planet Sci 34:263–291. https://doi.org/10.1146/annurev.earth.34.031405.125125

Matsushima T, Muramatsu D, Aizawa K, Shimizu H (2021) The geyser-like fluctuation of water level in hot spring pool at Iwo-Yama West Crater. In: Report of 148th Coordinating Committee for Prediction of Volcanic Eruption, JMA 1–2:36–39. (**in Japanese**) https://www.data.jma.go.jp/svd/vois/data/tokyo/STOCK/kaisetsu/CCPVE/shiryo/148/148_1-2.pdf

Mizutani H, Ishido T, Yokokura T, Ohnishi S (1976) Electrokinetic phenomena associated with earthquakes. Geophys Res Lett 3:365–368. https://doi.org/10.1029/GL003i007p00365

Muramatsu D, Matsushima T, Ichihara M (2021) Reconstructing surface eruptive sequence of 2018 small phreatic eruption of Iwo-Yama volcano, Kirishima Volcanic Complex, Japan, by infrasound cross-correlation analysis. Earth Planets Space 73:8. https://doi.org/10.1186/s40623-020-01344-6

Namiki A, Munoz-Saez C, Manga M (2014) El Cobreloa: a geyser with two distinct eruption styles. J Geophys Res Solid Earth 119:6229–6248. https://doi.org/10.1002/2014JB011009

Namiki A, Ueno Y, Hurwitz S, Manga M, Munoz-Saez S, Murphy F (2016) An experimental study of the role of subsurface plumbing on geothermal discharge. Geochem Geophys Geosyst 17:3691–3716. https://doi.org/10.1002/2016GC006472

Nishi Y, Ishido T, Sugihara M, Tosha T, Matsushima N, Scott B (2000) Monitoring of geyser activity in Whakarewarewa, New Zealand. In: Proceedings World Geothermal Congress 2000. pp 1509–1513. https://www.researchgate.net/publication/266072079

Nishimura T, Ichihara M, Ueki S (2006) Investigation of the Onikobe geyser, NE Japan, by observing the ground tilt and flow parameters. Earth Planets Space 58:21–24. https://doi.org/10.1186/BF03351967

Reed MH, Munoz-Saez C, Hajimirza S, Wu S, Barth A, Girona T, Rasht-Behesht M, White EB, Karplus MS (2021) The 2018 reawakening and eruption dynamics of Steamboat Geyser, the world's tallest active geyser. Proc Natl Acad Sci 118:e2020943118. https://doi.org/10.1073/pnas.2020943118

Revil A, A, Jardani A, (2013) The self-potential method: theory and applications in environmental geosciences. Cambridge University Press, Cambridge. https://doi.org/10.1017/CBO9781139094252

Revil A, Pezard PA, Glover PWJ (1999) Streaming potential in porous media 1. Theory of the zeta potential. J Geophys Res 104:20021–20031. https://doi.org/10.1029/1999jb900089

Scott BJ (1994) Cyclic activity in the crater lakes of Waimangu hydrothermal. Geothermics 23:555–572

Tajima Y, Matsuo Y, Shoji T, Kobayashi T (2014) Eruptive history of Ebinokogen volcanic area of Kirishima volcanoes for the past 15,000 years in Kyushu, Japan. Bull Volcanol Soc Jpn 59:55–75. https://doi.org/10.18940/kazan.59.2_55. (**in Japanese with English abstract**)

Tajima Y, Nakada S, Maeno F, Huruzono T, Takahashi M, Inamura A, Matsushima T, Nagai M, Funasaki J (2020) Shallow magmatic hydrothermal eruption in April 2018 on Ebinokogen Ioyama Volcano in Kirishima Volcano Group, Kyushu, Japan. Geosciences 10:183. https://doi.org/10.3390/geosciences10050183

Tajima Y, Matsushima T, Ishibashi J, Masuda H, Maeno F (2021) Geothermal activities around Iwo-Yama (Iwo-Yama, Iwo-Yama west fumarole area). Report of 149th Coordinating Committee for Prediction of Volcanic Eruption, JMA 3–5:50–55. (**in Japanese**) https://www.data.jma.go.jp/svd/vois/data/tokyo/STOCK/kaisetsu/CCPVE/shiryo/149/149_3-5.pdf

Toramaru A, Maeda K (2013) Mass and style of eruptions in experimental geysers. J Volcanol Geotherm Res 257:227–239. https://doi.org/10.1016/j.jvolgeores.2013.03.018

Tsukamoto K, Aizawa K, Chiba K, Kanda W, Uyeshima M, Koyama T, Utsugi M, Seki K, Kishita T (2018) Three-dimensional resistivity structure of Iwo-Yama volcano, Kirishima Volcanic Complex, Japan: Relationship to shallow seismicity, surface uplift, and a small phreatic eruption. Geophys Res Lett 45:12821–12828. https://doi.org/10.1029/2018GL080202

Vandemeulebrouck J, Stemmelen D, Hurst T, Grangeon J (2005) Analogue modeling of instabilities in crater lake hydrothermal systems. J Geophys Res Solid Earth 110:B02212. https://doi.org/10.1029/2003JB002794

Vandemeulebrouck J, Roux P, Cros E (2013) The plumbing of Old Faithful Geyser revealed by hydrothermal tremor. Geophys Res Lett 40:1989–1993. https://doi.org/10.1002/grl.50422

Vandemeulebrouck J, Sohn RA, Rudolph ML, Hurwitz S, Johnston MJS, Soule SA, McPhree D, Glen JMG, Karlstrom L, Murphy F, Manga M (2014) Eruptions at Lone Star Geyser, Yellowstone National Park, USA, Part 2: Geophysical constraints on subsurface dynamics. J Geophys Res 119:8688–8707. https://doi.org/10.1002/2014JB011526

Wendel J (2014) Yellowstone geysers influenced by internal processes. Eos Trans AGU 95:180. https://doi.org/10.1002/2014EO210008

Wu SM, Ward KM, Farrell J, Lin FC, Karplus M, Smith RB (2017) Anatomy of old faithful from subsurface seismic imaging of the Yellowstone Upper Geyser Basin. Geophys Res Lett 44:10240–10247. https://doi.org/10.1002/2017GL075255

Wu SM, Lin FC, Farrell J, Allam A (2019) Imaging the deep subsurface plumbing of Old Faithful geyser from low-frequency hydrothermal tremor migration. Geophys Res Lett 46:7315–7322. https://doi.org/10.1029/2018GL081771

Wu SM, Lin FC, Farrell J, Keller WE, White EB, Hungerford JD (2021) Imaging the subsurface plumbing complex of steamboat geyser and cistern spring with hydrothermal tremor migration using seismic interferometry. J Geophys Res Solid Earth 126:e2020JB021128. https://doi.org/10.1029/2020JB021128

Publisher's Note